Accelerated Determination of the S-N Curve for Fiber-reinforced Composites Using a Quasistatic Tri-modal Tensile Test System

Kundo Park[1], Antonio del Bosque[2,3], Alejandro Ureña[3,4], Grace X. Gu[5], Flavia Libonati[6,*], Seunghwa Ryu[1,*]

[1] Department of Mechanical Engineering, Korea Advanced Institute of Science and Technology, Daejeon, Republic of Korea
[2]Technology, Instruction and Design in Engineering and Education Research Group, Catholic University of Ávila, Ávila, Spain
[3]Research Group on Nano and Multifunctional Composites for Advanced Technologies, Escuela Superior de Ciencias Experimentales y Tecnología, Universidad Rey Juan Carlos, Móstoles (Madrid), Spain
[4]Instituto de Investigación de Tecnologías para la Sostenibilidad, Universidad Rey Juan Carlos, Móstoles (Madrid), Spain
[5]Department of Mechanical Engineering, University of California, Berkeley, CA 94720, USA
[6]Department of Mechanical, Energy, Management and Transportation Engineering, University of Genoa, Genova, Italy
[*] Co-corresponding Authors
flavia.libonati@unige.it
ryush@kaist.ac.kr

Abstract

Fatigue is one of the dominant modes of structural failure in materials across a wide spectrum of applications, from renewable-energy systems, transportation, and medical implants to the emerging category of flexible electronic devices. Yet, structural design for fatigue safety still lacks a reliable alternative for the conventional fatigue test, which demands numerous specimens and a vast number of loading cycles, making it very time- and cost-intensive, as well as resource-inefficient. In this study, we introduce a multiphysics material testing system, named the Tri-modal tensile test (T^3) system, capable of estimating the S-N curve of fiber-reinforced composites with just a single uniaxial tensile test. This testing system is built upon a uniaxial tensile test of Carbon nanotube-doped Glass fiber reinforced polymer (GFRP), during which changes in the internal damage state for the entire stress-strain levels are closely monitored through infrared thermography and electrical resistance measurements. The multiphysics signals obtained from the T^3 system are analyzed using damage and fatigue-related theories to derive a reliable estimation of the S-N curve. Then, we validate the proposed system by comparing the S-N curves estimated with the T^3 system to actual data points obtained from conventional fatigue tests, across three composite configurations featuring different laminate sequences: quasi-isotropic, angle-ply, and unidirectional. Results showed that the S-N curves estimated with our T^3 system align closely with the actual fatigue test results, highlighting the potential of the T^3 system as an accelerated and reliable method for evaluating the S-N curve of composite materials.

1. Introduction

While each loading cycle may seem benign, overlooking the silent accumulation of fatigue in material can trigger sudden, catastrophic failures. Fatigue failure is one of the dominant modes of structural breakdown in materials across a wide spectrum of applications, from aircraft, automotive, power generation systems, wearable devices, medical implants to the emerging category of flexible electronic devices. Yet, fatigue failure of materials is a highly non-linear mechanism driven by the interplay of multiple factors, including the applied stress ratio ($R = \sigma_{min} / \sigma_{max}$), stress concentrations, and various damage modes, making it challenging to develop a comprehensive theoretical model for predicting fatigue property (i.e., the S-N curve) [1-5]. This difficulty is particularly pronounced in composite materials due to their complex internal structures, making it very challenging to anticipate their fatigue property with theoretical means [6-9]. Consequently, engineers rely on experimentally determined S-N curves along with safety factors to predict service life and design fatigue-safe structures.

Conventional fatigue tests have been widely employed to determine a material's S-N curve. This classic method involves subjecting a material specimen to repetitive loading cycles, ranging from tens to million, to sample just one data point on the S-N curve. According to ASTM standard, typically 24 or more data points (thus, samples) are required to precisely represent the full S-N curve, necessitating significant investments of time and resources [10]. Due to this substantial burden associated with measuring fatigue property of materials, industries often resort to overdesign, using heavier and more expensive materials than necessary to reduce the risk of unexpected fatigue failures [11]. Such overdesign increases material consumption and structural weight in automotive applications, potentially raising energy consumption and thereby diminishing the benefits of lightweight composites. This challenge is also relevant to energy and sustainable infrastructure applications, where FRP composites are increasingly used in fatigue-critical and dynamic components such as wind-energy structures and composite pressure vessels for energy storage [12]. Furthermore, recent advances in machine learning-driven structural optimization have successfully enhanced static mechanical properties like Young's modulus, strength, and toughness. However, data-driven optimization of materials specifically for fatigue properties still remain out of reach because the fatigue property is extremely expensive-to-evaluate [13-16]. Therefore, there is a growing demand for an innovative method that can quickly and accurately assess the fatigue property of composite materials.

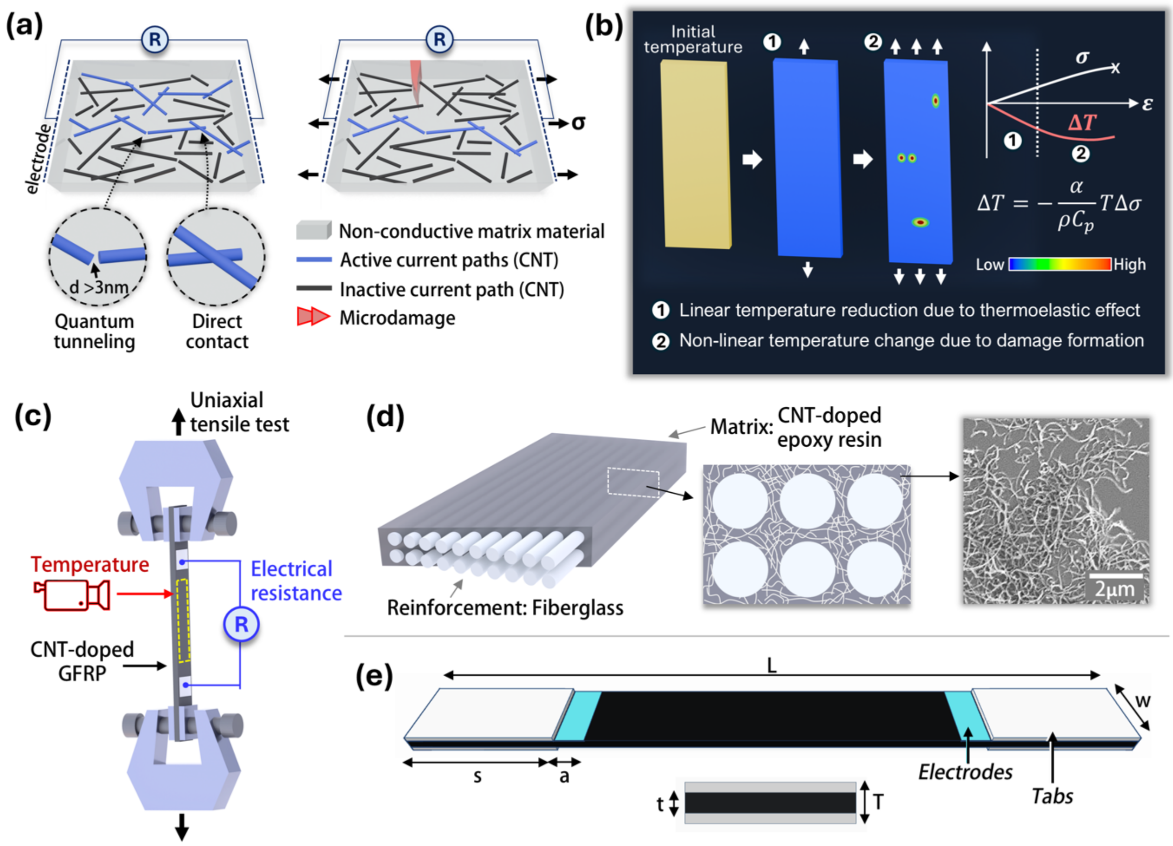

Figure 1. Fundamental principles and implementation of Tri-modal Tensile Test (T^3) system. (a) Monitoring of microdamage via electrical resistance measurement. (b) Monitoring of microdamage via IR thermography. (c) Schematic diagram of three-channel tensile test. (d) Schematic diagram of CNT-doped GFRP composite. (e) Geometry and dimensions of test samples (the values are provided in **Table 1**).

Length [mm]	L	s	a	w	T	t
Quasi-isotropic laminate [0/+45/90/-45]$_{2S}$	250	50	10	25	5.2	3.2
Angle-ply laminate [±45]$_{3S}$	250	50	10	25	4.4	2.4
Unidirectional [0]	250	56	10	15	3.6	1.6

Table 1. Geometrical dimensions of the test specimen.

There has been ongoing research focused on advanced methods to more rapidly assess the fatigue properties of materials, serving as alternatives to conventional fatigue testing. One of the earliest techniques in this regard is the high-frequency (ultrasonic) fatigue test [17-19]. An ultrasonic fatigue test uses very high-frequency vibrations (typically around 20 kHz) to explore the high cycle fatigue regime ($N > 10^6$) of the material, significantly shortening the testing time. However, the method may not accurately represent the fatigue behavior observed at lower frequencies, since the highly dynamic cyclic load can generate undesirable temperature increases, which can affect the mechanical properties of the matrix, and neglect the viscoelastic responses of the material, in case of a polymeric matrix. Meanwhile, other researchers, primarily highlighted by Ristano et al. who first applied the method to metals, tried to observe the thermal response of materials during fatigue or static tests, aiming to capture internal damage phenomena and utilize this information to estimate fatigue properties [20-23]. One well-known technique is the "stepwise" fatigue test, where multiple constant-amplitude loading blocks are applied in sequence, and the stabilization temperature for each block is measured [24-29]. The resulting temperature curve typically shows two distinct slopes, and the stress level at which the slope abruptly changes is taken as the material's fatigue limit. Another method proposed by Libonati et al. involves monitoring the initial temperature slope during a static test, identifying the stress level at which the early linearity in temperature ends - this point is taken as the fatigue strength of the material [22]. Although thermography-based methods significantly reduce both the number of samples and the testing time, the test still demands considerable time and can only determine the material's fatigue strength with limited accuracy. A combined approach coupling electrical resistance measurements and infrared (IR) thermography during static test has also been introduced, offering more precise prediction of the fatigue strength of composite materials [30]. Yet, no advanced method has been reported that can quickly predict the extensive S-N curve and completely replace the conventional fatigue test.

In this study, we introduce, for the first time, a multiphysics material testing system capable of rapidly estimating the S-N curve of fiber-reinforced polymer composites with just one quasistatic uniaxial tensile test. Here, this method is referred to as the Tri-modal Tensile Test (T^3) system. As the name indicates, this testing system is built upon a uniaxial tensile test of CNT-doped GFRP. This allows for closely monitoring, via IR thermography and electrical resistance measurements, changes in the internal damage state at entire stress-strain levels. The multiphysics signals, obtained from the testing system, are analyzed using damage and fatigue-related theories to derive a reliable estimation of the S-N curve. Then, we validate the proposed system by comparing the S-N curves obtained from the T^3 system with those obtained from conventional fatigue tests, performed on three composite configurations featuring different stacking sequences: quasi-isotropic, angle-ply, and unidirectional. To further understand the basis of the estimation, additional analysis is carried out, including mechanical hysteresis analysis, electrical resistance hysteresis analysis, and microscopic examination.

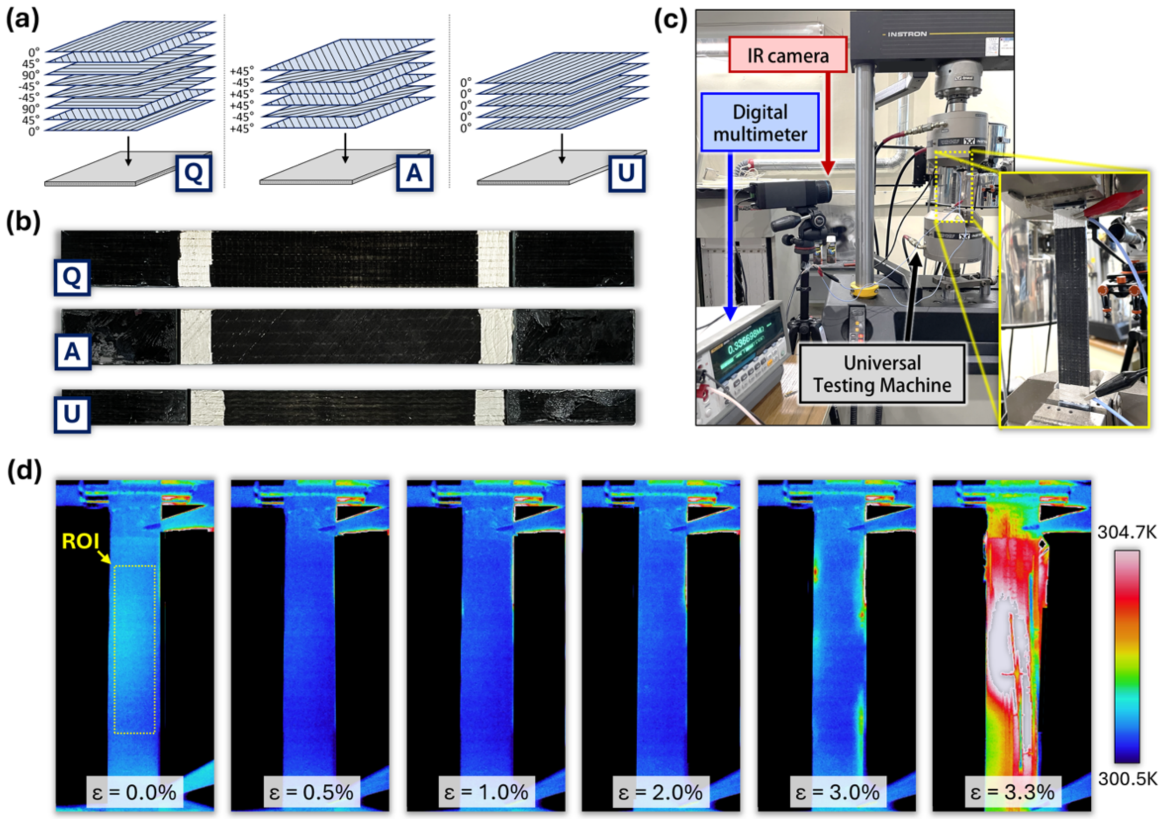

Figure 2. Test specimens and setup of the T^3 system. (a) The three different composite configurations analyzed: Q, quasi-isotropic, A, angle-ply, U, unidirectional. (b) Test specimens. (c) T^3 system setup. (d) Thermographic images taken at different instants during a tensile test.

2. Tri-modal Tensile Test (T^3) system

T^3 system is a multiphysics material testing system based on i) a uniaxial tensile test, ii) electrical resistance measurement, and iii) IR thermographic measurements, and it is proposed as an accelerated method to predict S-N curve of carbon nanotube (CNT)-doped GFRP composites (**Figure 1c** and **Figure 2c**). In this system, a CNT-doped GFRP composite material machined into a tensile specimen is mechanically tested under uniaxial tensile test at a constant crosshead speed. During the deformation process, two different in-situ damage monitoring methods (electrical resistance monitoring and IR thermography) are employed to capture the damage phenomena of the sample at different stress levels. Based on the three multiphysics signals acquired from the system, damage-related and fatigue-related theories are used to derive a reasonable estimation of the S-N curve.

Mechanical tests. Simple quasistatic uniaxial tensile tests are carried out on CNT-doped GFRP, following the standards ASTM D3039 (**Figure 1e, Figure 2b**) to determine the static mechanical performance and assess the different failure modes and damage propagation occurring in different types of composite configurations. Detailed information on the mechanical tensile test is provided in the **Experimental Section**.

Electrical resistance measurements. The first in-situ damage monitoring method adopted in this system is electrical resistance measurement, which is performed while each sample is subjected to loading. As depicted in **Figure 1a and d**, an electrically conductive network in a non-conductive composite material can be formed by dispersing a threshold amount of CNT during the fabrication stage, that is not affecting the overall mechanical properties of the composite. By evaluating the change in the electrical resistance of this CNT percolation network, which depends on the material deformation and the internal micro-defects, it is possible to evaluate the onset and the evolution of microdamage in the composite material [31-35].

IR thermographic measurements. The other damage monitoring method used in this system is IR thermography. Various thermo-mechanically coupled phenomena occurs in a composite material during the tensile test, such as the thermoelastic effect, evolution of micro defects, fiber–matrix detachment, and delamination, and these phenomena can be captured by IR thermography as variation of temperature as depicted in **Figure 1b** and **Figure 2d** [22, 36]. The thermoelastic effect is the reversible temperature change in a material caused by linear elastic deformation, due to the conversion between mechanical work and thermal energy. In the initial stage of deformation, the average temperature of the material declines linearly due to thermoelastic effect, indicating that the material is experiencing nearly reversible and elastic deformation [37]. At a stress level we call linearity threshold, σ_{lin}, the temperature graph starts to deviate from the initial linearity. Above this stress level, the temperature still displays a decreasing trend owing to the tensile thermoelastic effect; however, in addition, local heat is generated in the material by the formation of distributed micro damages within the matrix as well as by the frictional heating from the fiber–matrix slippage. Moreover, the local stress relaxation around the micro damage leads to an increase in the temperature around it.

Each of the three multiphysics signals from our proposed T^3 system provide crucial information needed for the estimation of the S-N curve of the material. The mechanical stress-strain curve allows us to determine the ultimate strength of the material, a stress level later used for $\sigma_{ult} = \sigma(N = 1)$ in S-N curve. The electrical resistance signal portrays the accumulation of irreversible damage inside the material, which is later used to determine the overall shape of the S-N curve. The IR thermography allows us to characterize the linearity threshold stress, a stress level which we will consider as fatigue strength $\sigma_{lin} = \sigma(N = 10^6)$ in S-N curve. In this study, we define the fatigue strength of GFRP at $N = 10^6$ cycles because 10^6 is widely used as practical high-cycle fatigue reference for polymer-matrix composites, where a distinct endurance limit is generally not observed.

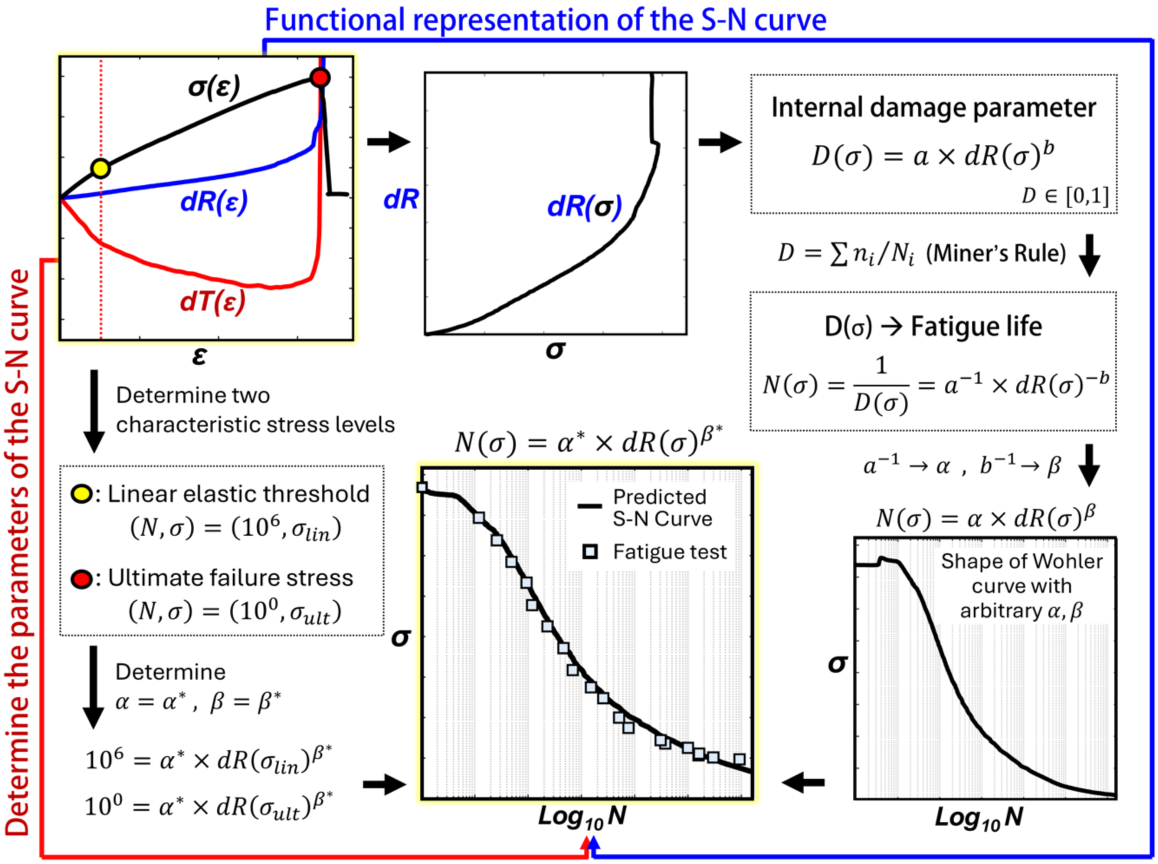

Figure 3. Overall workflow chart of using the result from T^3 system to estimate the S-N curve. The stress–strain and thermal responses are used to identify the two characteristic stress levels, the ultimate strength and linearity threshold, respectively. The electrical resistance response, interpreted as an internal damage parameter, determines the overall shape, or functional representation, of the S–N curve.

3. Estimation of S-N curve using data from the T^3 system

The three multiphysics signals (mechanical, electrical, and thermal) acquired from T^3 system are interpreted with fatigue-related theories to make a reasonable estimation of the S-N curve (**Figure 3**). The mathematical procedure can be divided into two main parts: (3.1) determination of overall S-N curve shape using electrical resistance signal and (3.2) fitting of the S-N curve using ultimate strength $\sigma_{ult} = \sigma(N = 1)$ and linearity threshold $\sigma_{lin} = \sigma(N = 10^6)$.

3.1 Determination of S-N curve shape using electrical resistance signal: functional representation of the S-N curve

First, the electrical resistance signal, which conveys the information of irreversible micro damage accumulation, is converted into a normalized damage parameter $d(\sigma) < [0, 1]$ that represents the cumulative fraction of fatigue life consumed. In this work, we adopt a functional form reported by Gao, L., et al., who experimentally related the electrical resistance evolution of a CNT percolation network to accumulation of internal damage within the FRP composite (quantified by the ratio of acoustic emission counts to the total acoustic emission counts recorded up to fracture). Their result revealed that the relationship between electrical resistance and the internal microdamage accumulation of GFRP composite during a quasi-static tensile test can be sufficiently represented with the following function form [38].

$$d(\sigma) = a\, dR(\sigma)^b \quad \text{(eq. 1)}$$

This relationship indicates that the electrical resistance response of the CNT percolation network and the accumulation of micro-damage within the composite during a quasistatic tensile test follows an exponential function. Here, the normalized damage parameter $d(\sigma) < [0, 1]$ is an indicator of the material's damage level or structural integrity, where $d = 1$ leads to the failure of material. The term $dR(\sigma)$ denotes the change in electrical resistance caused by internal damage development. The coefficient a and exponent b are unknown fitting parameters that depend on factors such as the material's characteristics, carbon nanotube (CNT) content, uniformity of CNT dispersion, resin type, and reinforcement content. The parameters will be determined in the next stage using the ultimate strength and linearity threshold stress of the material, both measured from T^3 system.

To further extend the formula to connect cyclic stress (σ) to fatigue life (N), to develop a S-N relationship, the damage parameter $d(\sigma)$ is then converted to fatigue life $N(\sigma)$ by using the Miner's rule [39]. Miner's rule is a linear cumulative damage model used in fatigue analysis, which states that failure occurs when the sum of the ratios of applied load cycles to the number of cycles to failure at each stress level reaches unity.

$$D = \sum_{i=1}^{k} \frac{n_i}{N_i} \quad \text{(eq. 2)}$$

Where D is the accumulated fatigue damage parameter, indicating that accumulation of fatigue damage up to $D = 1$ under varying cyclic loads leads to failure of sample. n_i is the number of cycles applied at stress level i. N_i is the number of cycles to failure at stress level i (from S-N curve), and k is the number of different stress levels. Although Miner's rule is originally formulated for cyclic loading conditions, its use here serves as a phenomenological bridge that links the normalized damage parameter obtained from a single quasi-static test to an equivalent fatigue life representation. Several studies have employed Miner's linear cumulative damage concept as a first-order approximation to connect monotonic or stepwise loading data with cyclic durability estimates, particularly when the damage parameter represents irreversible microstructural degradation measurable through electrical resistance [40-42].

By the introduction of Miner's rule, we can determine the number of cycles to failure (N_i) for a specific stress level (σ_i) by fusing the following relationship.

$$d(\sigma_i) = \frac{1}{N_i} \quad \text{(eq. 3)}$$

Here, $d(\sigma_i)$ is the normalized damage formed in the material when one cycle of load σ_i is applied to the material, which can be determined with the T^3 system using (eq. 1). N_i is the total number of cycles to failure at stress σ_i. By combining (eq. 1) and (eq. 3), we get a generalized equation that connects applied stress σ_i to number of cycles to failure N_i.

$$\frac{1}{N_i} = a\, dR(\sigma_i)^b \quad \text{(eq. 4)}$$

By inverting both sides, and replacing the unknown parameters a and b to $\alpha = a^{-1}$ and $\beta = -b$, respectively, we obtain:

$$N_i = \alpha\, dR(\sigma_i)^\beta \quad \text{(eq. 5)}$$

3.2 Fitting of the S-N curve using ultimate strength $\boldsymbol{\sigma_{ult} = \sigma(N = 1)}$ and linearity threshold $\boldsymbol{\sigma_{lin} = \sigma(N = 10^6)}$

In (eq. 5), two fitting parameters α and β, must be identified to fully define the relationship. Since there are two unknowns, basic mathematics dictates that two data points (σ_i, N_i) are required to determine them. From the T^3 system, the mechanical stress-strain curve provides one point $(N, \sigma) = (10^0, \sigma_{ult})$, while the temperature curve provides a second point $(N, \sigma) = (10^6, \sigma_{lin})$, each point indicated in red and yellow dots, respectively, in **Figure 3**.

The ultimate strength from the T^3 system represents the y-intercept of the S-N curve $(N, \sigma) = (10^0, \sigma_{ult})$, since the material can withstand only a single loading cycle at this stress level. The linearity threshold stress is defined as the stress level where the initially linear decrease in temperature shifts to a non-linear trend. At low stresses, the material undergoes reversible linear elastic deformation, causing a linear temperature drop due to the thermoelastic effect. Once the stress reaches the linearity threshold, irreversible micro-damage begins to develop within the material, introducing heat generation and resulting in a non-linear temperature response. Based on the assumption that cyclic loading associated with irreversible damage leads to a finite fatigue life ($N = 10^0 - 10^6$), whereas purely reversible elastic loading leads to an almost infinite fatigue life ($N > 10^6$), we can assign the point $(N, \sigma) = (10^6, \sigma_{lin})$ on the S-N curve. By applying (eq. 5) together with the two data points, we can uniquely solve for the values of α and β.

4. Results and discussion

Here we present the result of both T^3 system and conventional fatigue test conducted on three different laminate configurations: (4.1) Quasi-isotropic, (4.2) Angle-ply, and (4.3) Unidirectional laminate (**Figure 2a-b**). Additionally, mechanical hysteresis test, permanent electrical resistance change measurement, and scanning electron microscopy (SEM) is performed to evaluate the material's structural integrity at different stress levels and elucidate the mechanism by which the T^3 system can be used to estimate the material's S-N curve. More details are provided in the **Experimental Section**.

4.1 Quasi-isotropic laminate $[0/+45/90/-45]_{2S}$

Figure 4a presents the Tri-modal signals obtained with T^3 system performed on the CNT-doped GFRP composite with a quasi-isotropic laminate sequence. The stress–strain curve displays the characteristic brittle yet high-strength response of GFRP under uniaxial tension. Concurrently, the electrical resistance of the specimen gradually increases, primarily attributed to the progressive separation of adjacent CNTs within the percolated conductive network. At the first stage of loading, the electrical response exhibits an approximately linear behavior, dominated by direct contact conduction between adjacent CNTs within the percolated network. As the applied strain increases, electron tunneling mechanisms become dominant, leading to a nonlinear and approximately exponential increase in electrical resistance with applied strain. Such evolution in the electrical response reflects the real-time accumulation of microstructural damage within the material. Meanwhile, the specimen's temperature decreases under tensile loading due to the thermoelastic effect, with the curve showing an initial linear drop followed by a nonlinear trend once the stress surpasses the threshold level σ_{lin}. The linearity threshold stress is identified through a linearity analysis of temperature curve, in which the linear region is considered to end once the R^2 error falls below 0.9999. Detailed information on how the linearity threshold stress, σ_{lin}, is determined and the result of linearity analysis are presented at Section 1 (**Supporting**

Information).

Using the Tri-modal measurements and the two characteristic stress levels, $\sigma_{lin} = 37.1MPa$ and $\sigma_{ult} = 380.1MPa$, we estimated the S-N curve following the procedure described in **Section 3**. The resulting curve is shown in **Figure 4b**: the solid line represents the average S-N curve estimated from five different trials, and the shaded area indicates the upper and lower bound from these trials, and the square markers correspond to experimental data obtained from fatigue test. Conventional fatigue tests are conducted on the same specimens following the procedure described in the **Experimental Section**. The T^3 system measurements results and the corresponding S-N curves from the five trials are provided at Section 2 (**Supporting Information**). It is observed from **Figure 4b** that the S-N curve estimated from the T^3 system aligns closely with the actual fatigue test result, highlighting the potential of the T^3 system test as an accelerated and reliable method for evaluating the S-N curve of composite materials. The narrow width of the shaded region indicates the excellent precision of the estimation, confirming that all five trials produced S-N curves that closely agree with the actual fatigue test data.

The underlying mechanism of how our T^3 system can accurately estimate the S-N curve comes from its ability to precisely monitor and quantify the internal damage evolution at different stress levels. The three multiphysics components (mechanical, electrical, and thermal measurement) all convey crucial damage-stress information that is needed to reconstruct the estimated S-N curve. Firstly, the **electrical resistance measurement** of CNT percolation network embedded in the material provides a sensitive measure of material's internal damage state. By leveraging the result from existing research that electrical resistance and acoustic emission (a direct marker of micro-damage) are correlated in exponential function (eq. 1) under uniaxial tension, we map the electrical resistance change from the T^3 system into a normalized damage parameter $d(\sigma) \in [0,1]$, yielding a monotonic measure of internal damage. With the normalized internal damage quantified, Miner's cumulative damage rule allows us to map the normalized damage level to how many cycles of fatigue the material can withstand, allowing the estimation of the overall S-N curve shape (eq. 5). To completely define the S-N curve, the two unknown parameters are determined by leveraging the key damage information from **mechanical stress-strain data** $(\sigma_{ult}, N_{ult} = 10^0)$, and **temperature data** $(\sigma_{lin}, N_{lin} = 10^6)$.

To understand how efficient the T^3 system is at monitoring and evaluating the damage evolution at different stress levels, we performed various tests to understand the degree of internal damage at different load levels: mechanical hysteresis tests (**Figure 4c**), permanent electrical resistance change measurements (**Figure 4d**), and Scanning Electron Microscopy, SEM (**Figure 4e**). **Figure 4c** represents the elastic modulus change of the material in mechanical hysteresis tests: where the specimen is loaded and unloaded twice up to certain stress level. Stiffness reduction of a material is one of the indicators that represent its internal damage evolution [43, 44]. When the material is loaded only up to 50MPa which is close to the linearity threshold, the material did not exhibit any elastic modulus degradation in the next load cycle, indicating that the material undergoes nearly reversible deformation at the stress level near the linearity threshold, allowing for the material have nearly infinite fatigue life (N $\approx 10^6$). On the other hand, as higher stress level is forced to the material (200MPa and 370MPa), the material experienced 14.2% and 23.94% elastic modulus degradation, indicating that the material can only withstand finite fatigue cycles upon such damage-inducing stress levels. Indeed, the actual fatigue data shows that the material can only withstand about 200 and 3 cycles, under 200MPa and 370MPa cyclic loads, respectively.

The same conclusion can be drawn from the electrical resistance hysteresis analysis (**Figure 4d**), and SEM images (**Figure 4e**). After loading up to 50 MPa (stress level close to linearity threshold) and fully unloading, no permanent change in resistance is detected, indicating that the fully reversible deformation did not initiate irreversible damage or compromise structural integrity; the cross-sectional SEM likewise appears intact. In contrast, at higher peak stresses, 200 MPa and 370 MPa, residual electrical resistance increases of 0.97% and 6.17%, respectively, persist after unloading, evidencing irreversible damage. This resistance evolution results from the progressive reduction in the number of efficient conductive pathways within the CNT network, as micro-cracks and interfacial debonding interrupt contact points and increase tunneling distances, making the resistance growth approximately proportional to the loss of conductive paths. Thus, SEM images reveal widespread micro-damage throughout the sample and, at the highest stress, the onset of critical macro-damage. All in all, the hysteresis analysis and microscopic analysis demonstrate that the T^3 system efficiently characterize the linearity threshold and evaluate the damage evolution in the material.

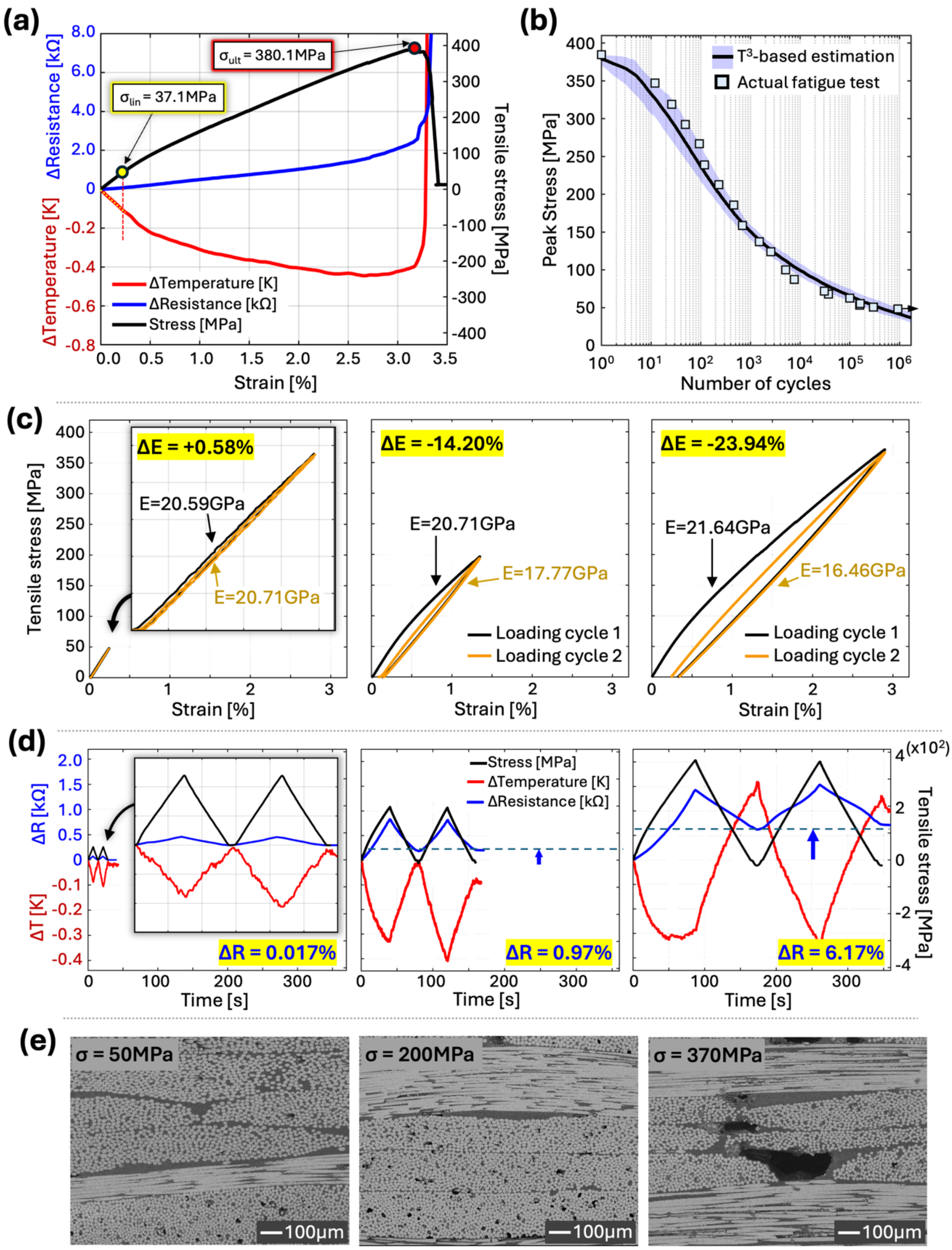

Figure 4. Result for [0/+45/90/-45]$_{2S}$ quasi-isotropic laminate. (a) Tri-modal signals obtained with T^3 system. (b) Comparison of predicted S-N curve and actual fatigue test data. (c) Elastic modulus degradation due to the formation of irreversible damage. (d) Permanent electrical resistance changes due to the formation of irreversible damage. (e) SEM images captured after the interrupted tensile test.

4.2 Angle-ply laminate [±45]$_{3S}$

Figure 5a shows the Tri-modal signals obtained with T^3 system for angle-ply laminate configuration.

Unlike the monotonic stress-strain curve of quasi-isotropic laminate configuration, the angle-ply laminate exhibit more bilinear trend, where the first stiff stage is a deformation mode where the overall structural integrity is maintained with minor micro-damages are nucleated, while the next low-stiffness stage accompanies structural disintegration such as delamination, fiber-matrix debonding, and crack propagation. As such heat generating damage phenomena arise early and strongly in this composite configuration, the temperature of specimen increases significantly during the tensile test.

It can be observed from the **Figure 5b** that the S-N curve estimated from the T^3 system aligns closely with the actual fatigue test result, highlighting the potential of the T^3 system as an accelerated and reliable method for evaluating the S-N curve of composite materials. The S-N curve is presented on a semi-log scale (linear stress amplitude S, logarithmic cycles to failure N) because fatigue life spans several orders of magnitude whereas the applied stress levels cover a comparatively limited range (from 0 to σ_{ult}). Regarding the stress levels chosen, because the S–N relation for composite fatigue is not known a priori for each laminate, a coverage-based sampling strategy was used. Stress levels were first distributed uniformly across the range (from 0 to σ_{ult}) to obtain a non-biased initial characterization, then enriched at lower stress amplitudes to ensure sufficient data density in the high-cycle regime (N>10^4), which is most relevant to fatigue-strength assessment.

To understand how efficient the T^3 system is at monitoring and evaluating the damage evolution at different stress levels, mechanical hysteresis test, permanent electrical resistance change measurement, and Scanning Electron Microscopy (SEM) are performed (**Figure 5c-e**). When a stress level below the linearity threshold (30MPa) is applied to the material, the material does not exhibit any elastic modulus degradation, permanent electrical resistance increase, and structural damage from microscopy. This indicates that the deformation occurs in a reversible manner, allowing for the material to withstand infinite fatigue life (N~10^6). On the other hand, when the stress above the linearity threshold (90MPa) is applied, the material exhibited significant stiffness degradation, noticeable permanent electrical resistance rise, and irreversible damages detected from microscopy. This indicates that the material can only withstand finite fatigue cycles upon such damage-inducing stress level. Indeed, the actual fatigue data shows that the material can only withstand about 500 cycles.

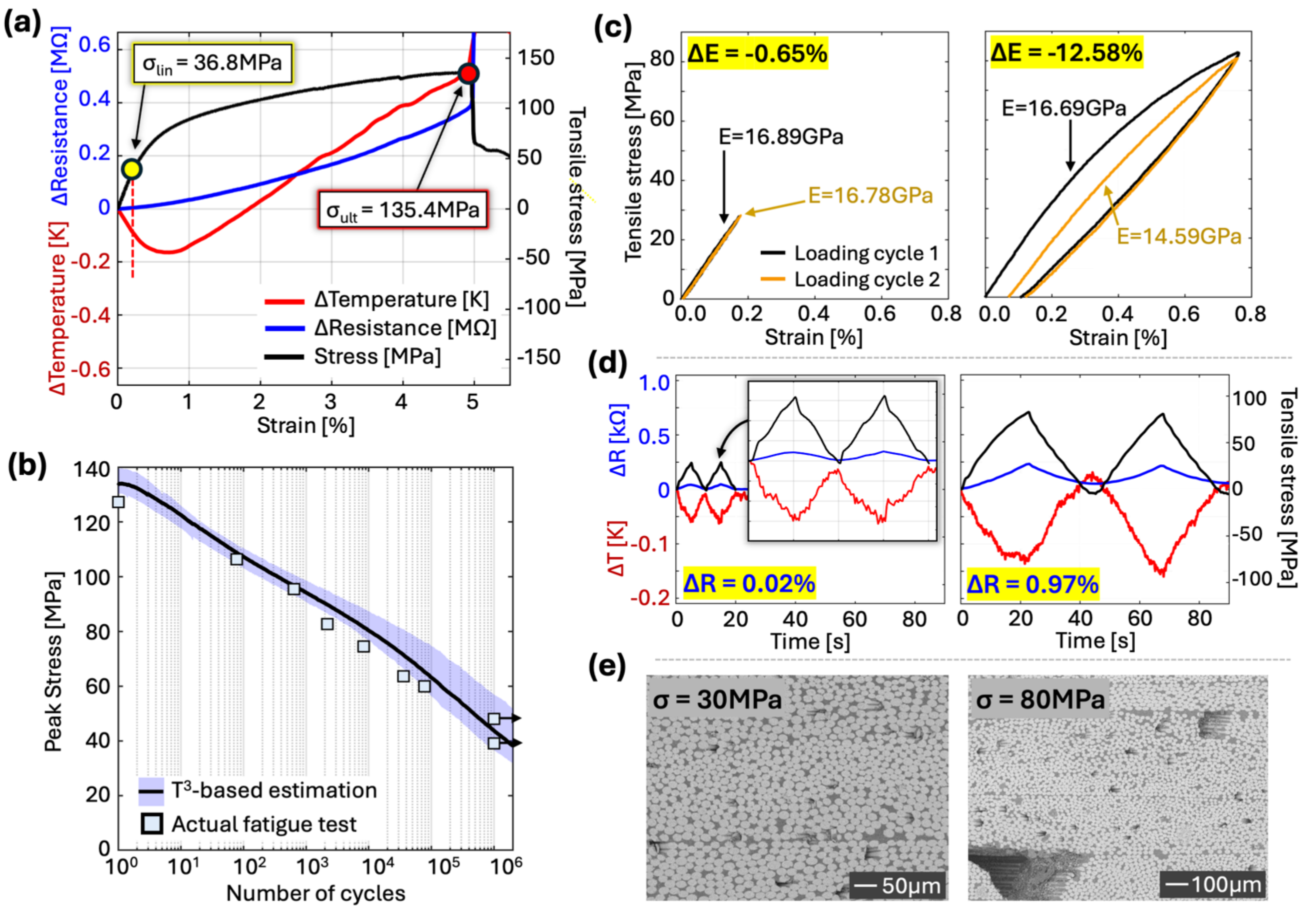

Figure 5. Result for $[\pm 45]_{3S}$ angle-ply laminate. (a) Tri-modal signals obtained with T^3 system. (b) Comparison of predicted S-N curve and actual fatigue test data. (c) Elastic modulus degradation due to the formation of irreversible damage. (d) Permanent electrical resistance changes due to the formation of irreversible damage. (e) SEM images captured after the interrupted tensile test.

4.3 Unidirectional laminate [0]

Figure 6a shows the Tri-modal signals obtained with T^3 system for unidirectional laminate configuration. The unidirectional laminate exhibit two stages with different deformation modes, where the first stage is a stiff deformation mode where the fibers aligned in the tensile direction are broken at low rate. Then in the second stage, when the structure reaches its ultimate strength, which primarily depends on the reinforcement content that slightly varies among the 5 trials, bundles of fibers start to rupture and the structural integrity of the specimen degrade significantly, leading to sudden increase in both temperature and electrical resistance.

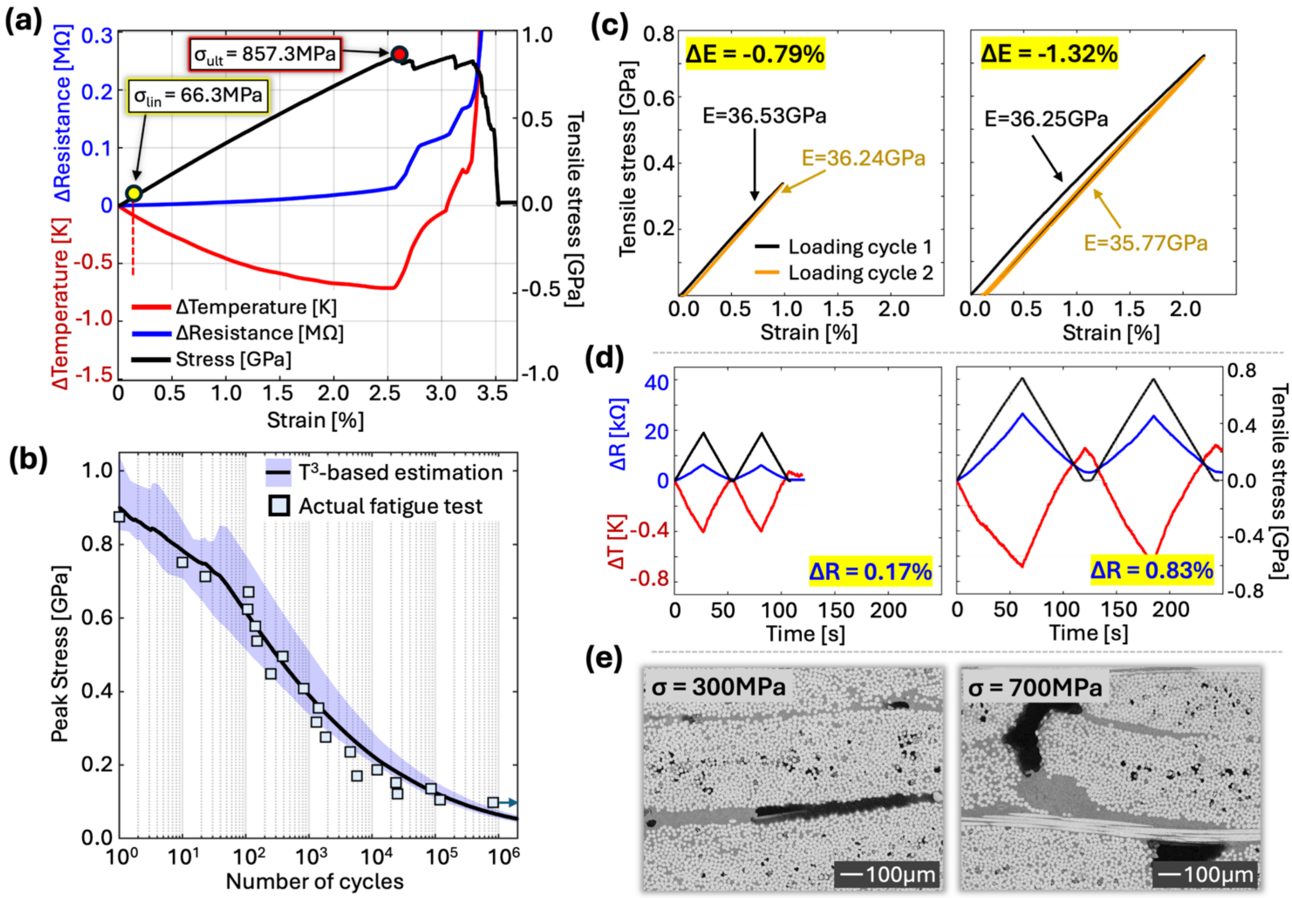

Figure 6. Result for [0] unidirectional laminate. (a) Tri-modal signals obtained with T^3 system. (b) Comparison of predicted S-N curve and actual fatigue test data. (c) Elastic modulus degradation due to the formation of irreversible damage. (d) Permanent electrical resistance changes due to the formation of irreversible damage. (e) SEM images captured after the interrupted tensile test.

It can be observed from the **Figure 6b** that the S-N curve estimated from the T^3 system aligns closely with the actual fatigue test result, highlighting the potential of the T^3 system as an accelerated and reliable method for evaluating the S-N curve of composite materials. However, compared to the other laminate configurations, the S-N curve estimation for unidirectional laminate configuration resulted in wider variance among the 5 trials conducted (shaded region). This is primarily because the transition from first deformation stage to the second stage vary among the samples by their reinforcement content, as even slight variation of reinforcement content may result in very significant difference in load bearing capacity in case of unidirectional fiber configuration. This variance highlights the advantage of our T^3 system. Unlike conventional methods that might average out these differences over dozens of samples, our system can detect batch to batch manufacturing variations (such as reinforcement content) within a single test.

To understand how efficient the T^3 system is at monitoring and evaluating the damage evolution at different stress levels, mechanical hysteresis test, permanent electrical resistance change measurements, and Scanning Electron Microscopy (SEM) are performed (**Figure 6c-e**). In case of unidirectional laminate configuration, the deformation exhibited gradual accumulation of matrix and fiber damage in the specimen. When a stress level of 300MPa is applied to the material, the material exhibited a minor elastic modulus degradation and small permanent electrical resistance increase, and structural damage from microscopy. This stress level allowed the specimen to withstand several thousands of load cycles in fatigue test. Even when much higher stress (700MPa) is applied, the material still exhibited gradual accumulation of local matrix and fiber damage, without sudden change of deformation mode or damage mode.

5. Conclusions

Evaluating fatigue properties has long been challenging because conventional fatigue testing demands numerous specimens and vast numbers of loading cycles, making it prohibitively time- and cost-intensive. In this study, we introduce, for the first time, a novel multiphysics material testing system, named T^3 system, capable of estimating the S-N curve of fiber-reinforced composites with just one uniaxial tensile test. This testing system is built upon a quasistatic uniaxial tensile test of CNT-doped GFRP, during which changes in the internal damage state at entire stress-strain levels are closely monitored through infrared thermography and electrical resistance measurements. The multiphysics signals obtained from the testing system are analyzed using damage and fatigue-related theories to derive a reliable estimation of the S-N curve. Then, we validate the proposed system by comparing the S-N curves estimated with the T^3 system with actual data points obtained from conventional fatigue tests, across three composite configurations featuring different stacking sequences: quasi-isotropic, angle-ply, and unidirectional. Result showed that the S-N curves estimated with T^3 system aligns closely with the actual fatigue test result, highlighting the potential of the T^3 system as an accelerated and reliable method for evaluating the S-N curve of composite materials. To further understand the basis of the estimation, various analysis is performed, including mechanical hysteresis analysis, electrical resistance hysteresis analysis, and microscopic examination. The analysis revealed that the underlying mechanism of how our T^3 system can accurately estimate the S-N curve comes from its ability to precisely monitor and quantify the internal damage evolution at different stress levels, allowing it for an efficient characterization of the linearity threshold stress and evaluation of the damage evolution in the material and finally, the reconstruction of the S-N curve from a single quasi-static tensile test. Our proposed method of measuring and converting the Tri-modal signals into a high-fidelity estimation of the S-N curve can significantly reduce the need for conventional fatigue test and accelerate the designing process of composite materials for fatigue-safety in various structural application. Ultimately, this framework suggests that fusing multiphysics signatures provides a pathway for fatigue life prediction across a broader class of functionalized engineering materials.

6. Experimental Section

Production of CNT-doped GFRP composites

We produce multiscale CNT-doped glass-fiber-reinforced polymer (GFRP) plates using a bi-component epoxy matrix (Araldite® LY 556, by Huntsman) combined with its hardener (XB 3473, by Huntsman) at a 100:23 ratio, and reinforce them with E-glass fibers (CASTRO composites) arranged in 3 different lay-up sequences: Quasi-isotropic $[0 /45 /90 /-45]_{2S}$, Angle-ply $[+-45]_{3S}$, and Unidirectional [0]. Nanocyl NC 7000 non-functionalized multiwall carbon nanotubes (MWCNTs, ~9.5 nm in diameter and up to 1.5 mm long) are dispersed within the epoxy matrix, establishing an electrically conductive network throughout the composite. MWCNT-epoxy dispersion is prepared with a step-wise calendaring procedure on an EXAKT 80E mini three-roll mill (Exakt Tech) following the optimized protocol reported in Ref. [45]. The CNT content is kept at 0.1 % wt., a concentration shown to provide high electrical sensitivity and sit slightly above the percolation threshold [46]. After mechanically dispersing the CNTs, the blend is degassed at 80 °C for 15 minutes to purge trapped air. The hardener is then mixed in, and the resulting resin is added to the glass-fiber preform. CNT-doped GFRP plates (210 mm x 297 mm) are fabricated via hand lay-up followed by hot pressing, and then cured for 8 hours at 140 °C.

Preparation of the test samples

The CNT-doped GFRP composite plates are cut into rectangular test specimens (dimensions specified in **Table 1**), as shown in **Figure 1e** and **Figure 2b**. An abrasive waterjet machine was employed for specimen preparation, ensuring precise dimensional accuracy and uniform cut surface finish. Specimen dimensions are determined according to ASTM D3479 and ASTM D3039 standards [10, 47]. End tabs were bonded to both ends of the specimens using 3M Scotch-Weld epoxy adhesive DP100, ensuring effective load transfer and preventing unintended fractures within the gripping region during tensile test. Electrically insulating material (polycarbonate) is chosen for the end tabs to prevent electrical conduction between the specimen and the grips of the testing machine. Additionally, electrodes are made at each end of the specimen by applying silver conductive paint, ensuring reliable electrical connectivity between the sample surface and the electrical wires.

Tri-modal tensile testing system

Uniaxial tensile tests are performed using a universal tensile testing machine (Instron 8801 with 100 kN load cell) under displacement control, with a crosshead speed of 2 mm/min and a data acquisition speed of 10 Hz. Throughout the tensile tests, the specimen surface is continuously monitored using an IR camera, capturing temperature changes during tensile loading, as illustrated in the experimental setup shown in **Figure 1c** and **Figure 2c**. A FLIR A655sc 25° thermal camera, capable of sensing mid-wave infrared (MWIR) radiation in the wavelength range of 7.5–14.0 μm with a thermal sensitivity of 30 mK, is used for thermography. Pixel-wise temperature data is acquired at a frequency of 50 Hz, and subsequently, the average temperature within the region of interest (ROI) is calculated using FLIR Thermal Studio Suite, a dedicated software tool for temperature field mapping. Electrical resistance changes in the specimen during tensile testing were tracked using a Fluke 8845A digital multimeter connected to real-time data logging software (FlukeView Forms), with measurements collected at 1 Hz. The recorded electrical signals were subsequently smoothed using a Savitzky-Golay finite impulse response (FIR) filter implemented in MATLAB.

Fatigue test

A fatigue testing system (Instron 8801) equipped with a servo-hydraulic actuator capable of applying cyclic forces up to ±100 kN is used. Hydraulic wedge grips are used to ensure secure and repeatable clamping of the specimen. Cyclic load is applied at a frequency of 3Hz, sufficiently low to prevent temperature buildup in the specimen. For the cyclic loading, a tension-tension loading condition with an R-ratio of $R = \sigma_{min}/\sigma_{max} = 0$ is selected in this study to maintain strict consistency with the T^3 system, which characterizes damage evolution under purely tensile loading. Using $R = 0$ avoids any compressive portion of the cycle and isolates tensile-driven damage mechanisms, enabling a direct mapping between this fatigue test and the structural health monitoring(SHM)-based damage metric obtained from the T^3 system. For each of the three laminate configurations, the ultimate strengths were identified through the T^3 system. Regarding the stress levels chosen, because the S–N relation for composite fatigue is not known a priori for each laminate, a coverage-based sampling strategy was used. Stress levels were first distributed uniformly across the range (from 0 to σ_{ult}) to obtain a non-biased initial characterization, then enriched at lower stress amplitudes to ensure sufficient data density in the high-cycle regime (N>10^4), which is most relevant to fatigue-strength assessment. All other fatigue test parameters adhered to the guidelines specified in ASTM D3479 (Standard Test Method for Tension-Tension Fatigue of Polymer Matrix Composite Materials) [47].

Interrupted uniaxial tensile tests

To investigate the internal damage state of the specimen at various load levels, mechanical hysteresis tests are conducted. In each test, the specimen is loaded to a predetermined load level, fully unloaded, and this loading-unloading sequence is repeated two times. In the interrupted tests, one stress level is selected near the linearity threshold, and significantly higher stress levels are also chosen to capture the phase of irreversible damage accumulation. During the test, the tri-modal measurement (stress, electrical resistance, and temperature) is performed, and the data is analyzed to assess mechanical hysteresis, and the permanent increase in electrical resistance. Additionally, the sample cross-sections were examined using Scanning Electron Microscopy (SEM).

Microscopic analysis

Scanning Electron Microscopy (SEM) is performed to observe the damage state of the samples following the interrupted tests. The samples are cut using an abrasive waterjet process, and their cross-sections are thoroughly polished using a series of circular sandpapers with progressively finer grit sizes (P100, P180, P320, P600, P1000). For this, a disc polishing machine is employed to eliminate micro-scratches and ensure a smooth cut surface. The polished surfaces are subsequently coated with a thin layer of gold via sputtering and examined using a Scanning Electron Microscope (JSM-IT800, JEOL USA). To enhance visualization of internal damage, SEM images were acquired using both backscattered and secondary electron imaging modes.

Acknowledgement

This work was supported by the Agencia Estatal de Investigación of the Spanish Government [Project MULTISENS PID2022-136636OB-I00]. G.X.G acknowledges support from the Alfred P. Sloan Foundation.

References

1. Reis, P.N.B., et al., *Fatigue life evaluation for carbon/epoxy laminate composites under constant and variable block loading.* Composites Science and Technology, 2009. **69**(2): p. 154–160. https://doi.org/10.1016/j.compscitech.2008.09.043
2. Alam, P., et al., *The fatigue of carbon fibre reinforced plastics-A review.* Composites Part B: Engineering, 2019. **166**: p. 555–579. https://doi.org/10.1016/j.compositesb.2019.02.016
3. Zhao, X., et al., *Fatigue behavior and failure mechanism of basalt FRP composites under long-term cyclic loads.* International Journal of Fatigue, 2016. **88**: p. 58–67. https://doi.org/10.1016/j.ijfatigue.2016.03.004
4. Bathias, C., *Fracture and fatigue of high performance composite materials: mechanisms and prediction.* Engineering fracture mechanics, 1991. **40**(4-5): p. 757–783. https://doi.org/10.1016/0013-7944(91)90234-R
5. Zhang, L., et al., *Fatigue failure mechanism analysis and life prediction of short fiber reinforced polymer composites under tension-tension loading.* International Journal of Fatigue, 2022. **160**: p. 106880. https://doi.org/10.1016/j.ijfatigue.2022.106880
6. Park, K., et al., *Designing staggered platelet composite structure with Gaussian process regression based Bayesian optimization.* Composites Science and Technology, 2022. **220**: p. 109254. https://doi.org/10.1016/j.compscitech.2021.109254
7. Park, K., et al., *Multi-objective Bayesian optimization for the design of nacre-inspired composites: optimizing and understanding biomimetics through AI.* Materials Horizons, 2023. **10**(10): p. 4329–4343. https://doi.org/10.1039/D3MH00137G
8. Deng, J., et al., *Review and assessment of fatigue delamination damage of laminated composite structures.* Materials, 2023. **16**(24): p. 7677. https://doi.org/10.3390/ma16247677
9. Guo, R., et al., *The fatigue performances of carbon fiber reinforced polymer composites–a review.* Journal of Materials Research and Technology, 2022. **21**: p. 4773–4789. https://doi.org/10.1016/j.jmrt.2022.11.053
10. *Standard Test Method for Tensile Properties of Polymer Matrix Composite Materials (ASTM D3039/D3039M-08)*. 2014, ASTM International.
11. Spillman Jr, W. *Fiber optic sensors for composite monitoring*. in *Fiber Optic Smart Structures and Skins*. 1989. SPIE. https://doi.org/10.1117/12.948882
12. Zhang, J., et al., *Past, present and future prospective of global carbon fibre composite developments and applications.* Composites Part B: Engineering, 2023. **250**: p. 110463. https://doi.org/10.1016/j.compositesb.2022.110463
13. Guo, K., et al., *Artificial intelligence and machine learning in design of mechanical materials.* Materials Horizons, 2021. **8**(4): p. 1153–1172. https://doi.org/10.1039/D0MH01451F
14. Jung, J., A. Chen, and G.X. Gu, *Aperiodicity is all you need: Aperiodic monotiles for high-performance composites.* Materials Today, 2024. **73**: p. 1–8. https://doi.org/10.1016/j.mattod.2023.12.015
15. Sharma, A., et al., *Advances in computational intelligence of polymer composite materials: machine learning assisted modeling, analysis and design.* Archives of Computational Methods in Engineering,

2022. **29**(5): p. 3341–3385. https://doi.org/10.1007/s11831-021-09700-9
16. Liang, Y., et al., *A review on recent applications of machine learning in mechanical properties of composites.* Polymer Composites, 2025. **46**(3): p. 1939–1960. https://doi.org/10.1002/pc.29082Digital
17. Fitzka, M., et al., *Usability of ultrasonic frequency testing for rapid generation of high and very high cycle fatigue data.* Materials, 2021. **14**(9): p. 2245. https://doi.org/10.3390/ma14092245
18. Apinis, R., *Accceleration of fatigue tests of polymer composite materials by using high-frequency loadings.* Mechanics of Composite Materials, 2004. **40**(2): p. 107–118. https://doi.org/10.1023/B:MOCM.0000025485.93979.dd
19. Backe, D., F. Balle, and D. Eifler, *Fatigue testing of CFRP in the Very High Cycle Fatigue (VHCF) regime at ultrasonic frequencies.* Composites Science and Technology, 2015. **106**: p. 93–99. https://doi.org/10.1016/j.compscitech.2014.10.020
20. Fargione, G., et al., *Rapid determination of the fatigue curve by the thermographic method.* International Journal of Fatigue, 2002. **24**(1): p. 11–19. https://doi.org/10.1016/S0142-1123(01)00107-4
21. La Rosa, G. and A. Risitano, *Thermographic methodology for rapid determination of the fatigue limit of materials and mechanical components.* International Journal of Fatigue, 2000. **22**(1): p. 65–73. https://doi.org/10.1016/S0142-1123(99)00088-2
22. Libonati, F. and L. Vergani, *Damage assessment of composite materials by means of thermographic analyses.* Composites Part B: Engineering, 2013. **50**: p. 82–90. https://doi.org/10.1016/j.compositesb.2013.01.012
23. Vergani, L.M., C. Colombo, and F. Libonati, *A review of thermographic techniques for damage investigation in composites.* FRATTURA E INTEGRITÀ STRUTTURALE, 2014. **8**(27): p. 1–12. https://doi.org/10.3221/IGF-ESIS.27.01
24. Risitano, A. and G. Risitano, *Determining fatigue limits with thermal analysis of static traction tests.* Fatigue & Fracture of Engineering Materials & Structures, 2013. **36**(7): p. 631–639. https://doi.org/10.1111/ffe.12030
25. Colombo, C., F. Libonati, and L. Vergani, *Fatigue damage in GFRP.* International Journal of Structural Integrity, 2012. **3**(4): p. 424–440. https://doi.org/10.1108/17579861211281218
26. Colombo, C., et al., *Fatigue behaviour of a GFRP laminate by thermographic measurements.* Procedia Engineering, 2011. **10**: p. 3518–3527. https://doi.org/10.1016/j.proeng.2011.04.579
27. Santonocito, D., et al., *Fatigue damage assessment in AM polymers evaluating their energy release.* Procedia Structural Integrity, 2021. **34**: p. 211–220. https://doi.org/10.1016/j.prostr.2021.12.031
28. Wei, W., et al., *A review of fatigue limit assessment using the thermography-based method.* Metals, 2024. **14**(6): p. 640. https://doi.org/10.3390/met14060640
29. Azizian-Farsani, E., et al., *On the optimization of fatigue limit in additively manufactured fiber reinforced polymer composites.* Progress in Additive Manufacturing, 2025: p. 1–20. https://doi.org/10.1007/s40964-025-00961-5
30. Park, K., et al., *Coupled health monitoring system for CNT-doped self-sensing composites.* Carbon, 2020. **166**: p. 193–204. https://doi.org/10.1016/j.carbon.2020.04.060

31. Thostenson, E.T. and T.W. Chou, *Carbon nanotube networks: sensing of distributed strain and damage for life prediction and self healing.* Advanced Materials, 2006. **18**(21): p. 2837–2841. https://doi.org/10.1002/adma.200600977
32. Fernandez Sanchez-Romate, X.X., et al., *Carbon nanotube-doped adhesive films for detecting crack propagation on bonded joints: a deeper understanding of anomalous behaviors.* ACS applied materials & interfaces, 2017. **9**(49): p. 43267–43274. https://doi.org/10.1021/acsami.7b16036
33. Picot, O.T., et al., *Using graphene networks to build bioinspired self-monitoring ceramics.* Nature communications, 2017. **8**(1): p. 14425. https://doi.org/10.1038/ncomms14425
34. Matos, M.A., et al., *Predictions of the electro-mechanical response of conductive CNT-polymer composites.* Journal of the Mechanics and Physics of Solids, 2018. **114**: p. 84–96. https://doi.org/10.1016/j.jmps.2018.02.014
35. Sánchez-Romate, X.F., et al., *Fatigue crack growth identification in bonded joints by using carbon nanotube doped adhesive films.* Smart Materials and Structures, 2020. **29**(3): p. 035032. https://doi.org/10.1088/1361-665X/ab7109
36. Harizi, W., et al., *Mechanical damage assessment of Glass Fiber-Reinforced Polymer composites using passive infrared thermography.* Composites Part B: Engineering, 2014. **59**: p. 74–79. https://doi.org/10.1016/j.compositesb.2013.11.021
37. Wong, A., J. Sparrow, and S. Dunn, *On the revised theory of the thermoelastic effect.* Journal of Physics and chemistry of solids, 1988. **49**(4): p. 395–400. https://doi.org/10.1016/0022-3697(88)90099-6
38. Gao, L., et al., *Coupled carbon nanotube network and acoustic emission monitoring for sensing of damage development in composites.* Carbon, 2009. **47**(5): p. 1381–1388. https://doi.org/10.1016/j.carbon.2009.01.030
39. Shimokawa, T. and S. Tanaka, *A statistical consideration of Miner's rule.* International Journal of Fatigue, 1980. **2**(4): p. 165–170. https://doi.org/10.1016/0142-1123(80)90044-4
40. Batsoulas, N.D. and G.I. Giannopoulos, *Cumulative fatigue damage of composite laminates: engineering rule and life prediction aspect.* Materials, 2023. **16**(8): p. 3271. https://doi.org/10.3390/ma16083271
41. D'Amore, A. and L. Grassia, *The Fatigue Response's Fingerprint of Composite Materials Subjected to Constant and Variable Amplitude Loadings.* Journal of Composites Science, 2023. **8**(1): p. 11. https://doi.org/10.3390/jcs8010011
42. Kassapoglou, C., *Fatigue of composite materials under spectrum loading.* Composites Part A: Applied Science and Manufacturing, 2010. **41**(5): p. 663–669. https://doi.org/10.1016/j.compositesa.2010.01.016
43. Talreja, R., *Transverse cracking and stiffness reduction in composite laminates.* Journal of composite materials, 1985. **19**(4): p. 355–375. https://doi.org/10.1177/002199838501900404
44. Hashin, Z., *Analysis of stiffness reduction of cracked cross-ply laminates.* Engineering Fracture Mechanics, 1986. **25**(5-6): p. 771–778. https://doi.org/10.1016/0013-7944(86)90040-8
45. Jiménez-Suárez, A., et al., *The influence of mechanical dispersion of MWCNT in epoxy matrix by calendering method: Batch method versus time controlled.* Composites Part B: Engineering, 2013.

48: p. 88–94. https://doi.org/10.1016/j.compositesb.2012.12.011
46. Sánchez-Romate, X.F., et al., *Novel approach to percolation threshold on electrical conductivity of carbon nanotube reinforced nanocomposites.* Rsc Advances, 2016. **6**(49): p. 43418–43428. https://doi.org/10.1039/C6RA03619H
47. *Standard Test Method for Tension-Tension Fatigue of Polymer Matrix Composite Materials (ASTM D3479/D3479M-19)*. 1976, ASTM International.